Interconnected Autonomous ac Microgrids via Back-to-Back Converters—Part II: Stability Analysis

Mobin Naderi, *Student Member, IEEE*, Yousef Khayat, *Student Member, IEEE*, Qobad Shafiee, *Senior Member, IEEE*, Tomislav Dragičević, *Senior Member, IEEE*, Hassan Bevrani, *Senior Member, IEEE*, and Frede Blaabjerg, *Fellow, IEEE*

***Abstract*—In this article, the stability of voltage source converter-based autonomous ac microgrids (MGs), which are interconnected through back-to-back converters (BTBCs), is analyzed. The small-signal stability analysis is based on a detailed, comprehensive and generalized small-signal modeling of the ac interconnected MGs (IMGs), which is possible for any number of MGs and interconnections. The large-signal stability of the IMGs is investigated for the case of the initial BTBC dc voltage as a part of paper contribution. A new margin/criterion is determined for the initial dc voltage in different situations of the BTBC operation. According to the proposed criterion, a fundamental difference between very weak MGs and conventional strong grids in the BTBC voltage stability is addressed. Using eigenvalue analysis and participation matrix, the main participating state variables and corresponding parameters in the dominant critical modes are recognized for an equilibrium point. Sensitivity analysis involves changing initial values of the state variables, parameters, and forcing functions to study their different values and find acceptable ranges of the parameters. Particularly, the considerable contribution of the BTBC in the critical modes is found out by analyzing the initial dc voltage, dc voltage controller and PLLs. In order to observe possible unstable situations and verify the transient studies, real-time simulations are provided for two and three MGs interconnected through BTBCs using OPAL-RT digital simulator. The IMGs can be robustly stable only by specifying the stabilizing ranges of the sensitive parameters to the critical modes and selecting their appropriate values.**

***Index Terms*—Back-to-back converters, dominant critical modes, interconnected ac microgrids, large-signal stability, sensitivity analysis, small-signal stability.**

I. Introduction

MICROGRIDS have demonstrated the ability to securely operate a set of distributed energy resources (DERs) and increase the renewable energy penetration in the conventional power systems [1]–[3]. They have also improved the supply reliability for the end-use loads in the islanded mode [4], [5]. Furthermore, microgrids (MGs) can be interconnected together to more improve reliability, resiliency, flexibility, sustainability and provide supporting inertia [1], [6]–[8]. AC interconnected microgrids (IMGs) can be constructed either from a number of autonomous MGs for the sake of MG shortage compensation [9]–[13], or from a distribution network due to critical conditions [6], [8], [14]–[16].

Although circuit breakers are usually used for interlinking ac IMGs [8], [11], [14], [15], back-to-back converters (BTBCs) are more flexible interfaces, which result in a separate frequency control of MGs [10], [13], [17]–[20]. Generally speaking, the control and operation of BTBC-IMGs are similar to the multi-area power systems inter-tied through high-voltage dc [20]–[22]. Both systems similarly lead to frequency stability improvement due to eliminating inter-area frequency interactions. However, the voltage strength of the two systems is different. In each area of the conventional power system, many synchronous generators participate in the load supply and inertia support. Furthermore, common load changes are less than 5% of the total supplied load [23]. Therefore, ac voltage of each area is stiff. On the contrary, MG's DERs are mostly inertia-less voltage source converter (VSC)-based units and have a considerable contribution in the load supply. In addition, load steps can be larger than 20% of the total MG load [6]. Hence, each DER outage or load change has a remarkable impact on the MG voltage/frequency, which means a weak grid. Broadly, the ac system weakness is expressed by the short circuit ratio (SCR), which is the ratio of the ac system three-phase short-circuit MVA to the exchanged dc power. The SCR of very weak grids is less than 2 [24]. The transient stability of interlinked weak grids via BTBCs has been investigated [25]–[27]. In such power systems, the BTBC power transfer limit is considered as a stability criterion.

Transient stability of the power system can be analyzed in four general methods, including time-domain, graphical, direct and automatic learning methods [28]. The graphical methods consists of equal-area criterion and phase portrait mostly used in one-machine systems [29]. The direct method employs Lyapunov functions, which is more applicable for low/reduced-order systems [8], [30]. The automatic learning methods benefit from intelligent algorithms such as artificial neural networks to assess transient stability [31]. Usual time-domain assessment

Manuscript received February 5, 2020; accepted April 3, 2020. Date of publication April 12, 2020; date of current version July 20, 2020. This work was supported by the Reliable Power Electronic based Power System (REPEPS) Project under the Villum Investigator Program funded by the Villum Foundation under Grant 25920. Recommended for publication by Associate Editor G. Oriti. *(Corresponding author: Mobin Naderi.)*

Mobin Naderi, Yousef Khayat, Qobad Shafiee, and Hassan Bevrani are with the Smart/Micro Grids Research Center (SMGRC), University of Kurdistan, Sanandaj 66177-15175, Iran (e-mail: m.naderi@eng.uok.ac.ir; y.khayat@eng.uok.ac.ir; q.shafiee@uok.ac.ir; bevrani@eng.uok.ac.ir).

Tomislav Dragičević is with the Technical University of Denmark, Copenhagen 2800, Denmark (e-mail: tomdr@elektro.dtu.dk).

Frede Blaabjerg is with the Department of Energy Technology, Aalborg University, Aalborg 9220, Denmark (e-mail: fbl@et.aau.dk).

Color versions of one or more of the figures in this article are available online at https://ieeexplore.ieee.org.

Digital Object Identifier 10.1109/TPEL.2020.2986695

criteria are the critical clearing time (CCT) and the power transfer limit (PTL) [25], [26], [32]. In general, the time-domain methods have been used for MG/IMG transient stability analysis [32], [33], however Lyapunov function [8], bifurcation theory [34], and unsymmetrical fault analysis [35] have been utilized rarely. Another common transient stability assessment method is sensitivity analysis, which is realized by changing the equilibrium point, i.e. parameters or initial values, based on the linearized state space model for systems with low nonlinearity degree, and the nonlinear model for even highly nonlinear systems [28].

The small-signal and transient stabilities of IMGs via circuit breakers (CB-IMGs) have been analyzed in the literature [8], [11], [12], [14], [15], [36]–[39]. An eigen-analysis method is presented in order to determine the suitable range of control parameters for IMG's DERs and to guarantee the IMG stability employing the sensitivity analysis [36]. In [37], the impact of rating/number of DERs and loads, as well as the autonomous MG topology on the IMG stability is investigated. Similar stability analysis is performed to study the impact of different interconnecting points within a distribution network on the IMG formation [14]. Parameter stability margins are also calculated using sensitivity analysis. In a more general method, a parametric criterion for IMG stability is achieved by applying Lyapunov stability on the simplified droop-based IMG model [8],[38]. In contrast, a detailed small-signal model of PV-based IMGs is proposed considering the dynamics of the PV controllers and dc sides [12]. Then, sensitivity analysis is employed to find acceptable parameter ranges affecting the dominant critical modes (DCMs). In [11], authors have presented a two-layer, four-level distributed control strategy for IMGs, then its impact on the small-signal stability is analyzed. Similar work has been presented for a distributed voltage control and power management of IMGs [15]. Authors have simplified the MG model with primary and secondary controllers and have studied their impacts on the IMG small-signal stability.

Stability analysis of BTBC-IMGs is evaluated in [10], [39], [40]. In [10], A specific configuration of MGs is considered in which any autonomous MG has a STATCOM/ESS unit to coordinate its generation with BTBC power exchange. A robust distributed controller is presented for such BTBC-IMGs to damp the oscillatory modes due to interaction of local DER controllers and make the system robust against the parametric uncertainties. A common structure of two autonomous ac MGs interconnected by a BTBC is considered to prove IMG frequency support [40]. Then, time-domain frequency stability analysis is conducted, which shows the frequency independence for BTBC-IMGs during faults. In [39], multiple MGs connected to a strong grid are studied, where the main IMG challenges, e.g. power exchanging do not reveal.

This article presents the stability assessment for ac BTBC-IMGs in the absence of a stiff grid, including both small-signal and transient stability analyses. Following features draw a clear distinction between this article and existing works.

1) A detailed and comprehensive modeling method is used for IMGs, which can be generalized for any number of MGs. The details of the comprehensive modeling is presented in the Part I of [41].
2) In the deployed small-signal and transient stability assessments for the IMGs, BTBCs are included as flexible interlinking devices, unlike the existing works in the literature [8], [10]–[12], [14], [15], [36], [37]. The corresponding challenges are introduced using analysis tools, e.g. sensitivity analysis to be more taken into account in future studies including stability analysis and controller design.
3) A transient stability assessment for the BTBC dc voltage, during enabling BTBC to exchange power, is developed based on the energy concept. Minimum stabilizing dc voltage criterion (MSDVC) for BTBC-included weak power grids/MGs is proposed as a criterion of time-domain methods. Different aspects of this issue are investigated, e.g. the impact of BTBC power flow direction on the transient stability.
4) MSDVC is a powerful transient stability margin for the case of enabling BTBC to exchange power as the large-signal disturbance. However, the common PTL criterion for HVDC/BTBC [25], [26], [32] is used in the case of faults as the large-signal disturbances. Nevertheless, an initial PTL is introduced, which is strongly correlated with MSDVC. Considering the MSDVC allows the BTBC to exchange any power level less than the power rating without instability. Whereas, the initial PTL leads to the same result with a different method.
5) Similar to [25]–[27], [42], the role of grid strength on the BTBC stability is discussed. However, in this paper, fully VSC-based very weak IMGs are taken into account, which causes a different phenomenon with respect to strong multi-area power systems, i.e. initial dc voltage transient instability for BTBCs.

The rest of this article is organized as follows. The summary of the proposed IMG modeling method, depicted in Part I [41], is addressed in Section II. Section III presents the transient stability analysis for the BTBC dc -link voltage. Verifying simulation results for small-signal and transient stability analyses are reported in Section IV, including sensitivity analysis and time-domain outputs, respectively. Finally, Section V concludes this article.

II. Small-Signal Modeling of Interconnected Microgrids

A general configuration of ac IMGs comprised of autonomous MGs, ac and dc interlinking lines (ILs), and interconnecting BTBCs is shown in Fig. 1. In the proposed modeling presented in Part I [41], each main module is modeled separately using a state space representation as

$$\dot{X}_M^k = A_M^k X_M^k + B_M^k U_M^k \tag{1}$$

$$Y_M^k = C_M^k X_M^k + D_M^k U_M^k \tag{2}$$

where X_M^k is the state vector of the k'th IMG module, i.e.,

$$X_M^k \subseteq \left\{ X_{\mathrm{MG}}^1, ..., X_{\mathrm{MG}}^n, ..., X_{IL}^{ij}, ..., X_B^{ij}, ... \right\} \tag{3}$$

where U_M^k is the input vector of k'th module determined based on all electrical/control interconnections from other modules. Y_M^k is all required connections to other modules. The matrices can be calculated for each module according to its components.

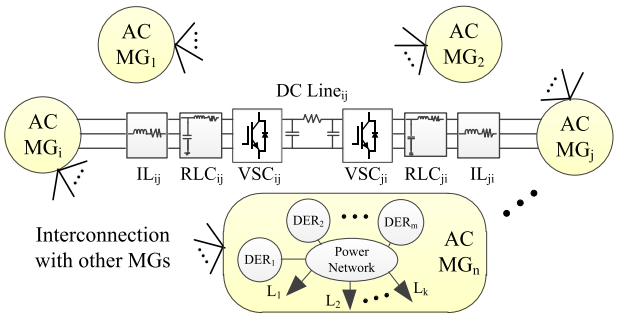

Fig. 1. General structure of interconnected ac MGs through back-to-back converters, dc and ac interlinking lines.

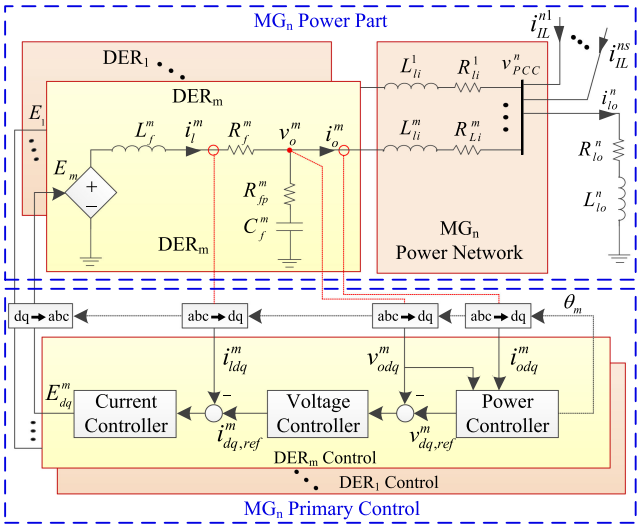

Fig. 2. General structure of autonomous ac MGs, including power part, and primary control modules.

A. Microgrid Modeling

Fig. 2 shows a general structure for autonomous ac MGs. The power part of the typical MG_n consists of m DERs, m ac lines as power network and a lumped RL load. The DERs are assumed as ideal averaging modeled VSCs series with RLC filters. The power network is modeled by series RL branches, which for weak grids $X/R < 1$ or $X/R \approx 1$.

For the sake of individual control of MGs, a primary control level is considered, including $\omega - P$ and $v - Q$ droop characteristics, and voltage and current controllers. The droop loops try to share the active/reactive powers among DERs and stabilize the frequency/voltage during disturbances. The voltage control regulates the output DER voltage. The current control is employed to limit the output current of each DER to the converter rating. Due to this necessary duty, MGs are generally very weak grids having an SCR < 2.

In the modeling method, all mentioned MG components are modeled independently by a state space representation. Then, one can find the overall MG model by interconnecting these partial models exploiting Robust Control Toolbox in MATLAB [41]. Therefore, IMGs with any number and different structures of MGs can be modeled.

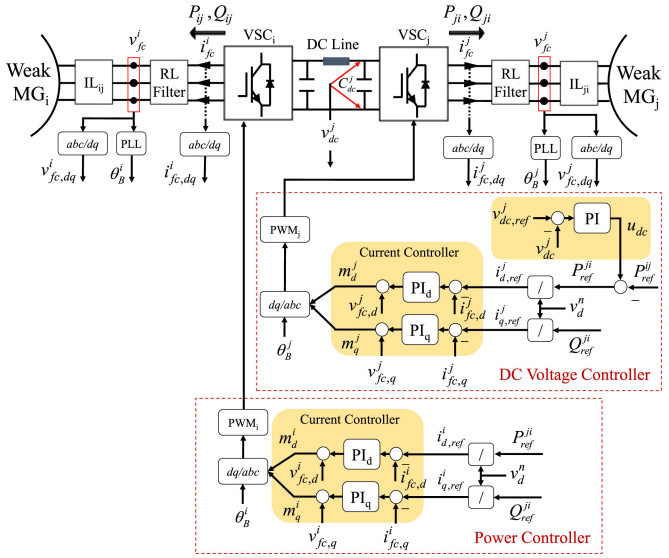

Fig. 3. Conventional PI controller-based power flow control of interlinking back-to-back converters, comprising power and dc voltage controllers.

B. Modeling of ac/dc Interlinking Lines

Ac interlinking lines are considered as series RL branches, as shown in Fig. 1, due to their low/medium lengths and dc lines are assumed to be resistive branches. Based on the BTBC position, two ac lines, each one between a MG and the BTBC, and one dc line between the BTBC's VSCs can be considered. The ac lines are modeled as separate IMG modules, however, the resistive dc line is included in the BTBC model.

C. Back-to-Back Converter Modeling

In order to exchange power between two ac MGs using a BTBC, a power controller and a dc voltage controller should be employed for the BTBC in addition to the individual MG controllers. As shown in Fig. 3, the power controller receives $P^{ij}_{\rm ref}/Q^{ij}_{\rm ref}$ from the global control level in coordination with both sender and receiver MGs, and tries to exchange it by controlling the VSC_i current. The dc voltage controller stabilizes the dc side voltage $V^j_{\rm dc}$ by regulating the VSC_j current. Moreover, it should pass the scheduled power forced by VSC_i through VSC_j. Two phase-locked loops (PLLs) are needed to synchronize the ac sides with the MGs.

The detailed dynamic models of the BTBC modules are obtained individually, then the overall BTBC model can be obtained by interconnecting all sub models [41].

D. Overall Model of Interconnected Microgrids

By modeling IMG modules separately, comprising MGs, BTBCs and interlinking lines, modeling of various IMG structures with any number of MGs is possible. The proposed modeling method based on sub-models and their interconnections leads to a comprehensive and generalized model for BTBC-IMGs. The IMG state space can be represented as

$$\dot{X}_{\rm IMG} = A_{\rm IMG} X_{\rm IMG} \tag{4}$$

where $X_{\rm IMG}$ is the overall state vector as

$$X_{\rm IMG} = \left[\overbrace{X^1_{\rm MG} \dots X^n_{\rm MG}}^{\rm MGs} \overbrace{\dots X^{ij}_{IL} \dots}^{\rm ILs} \overbrace{\dots X^{ij}_{B} \dots}^{\rm BTBCs}\right]^T.$$

$A_{\rm IMG}$ can be computed for interconnecting the desired number of MGs, interlinking lines and BTBCs using appropriate functions in Robust Control Toolbox [41].

III. Transient Stability of Back-to-Back Converter DC Voltage

According to the results of eigenvalue analysis and participation matrix presented in Part I [41], BTBC dc voltage and its controller are much effective on the IMG small-signal stability. In this section, we want to theoretically prove that this impact is also on the transient stability. Here, large power flow changes are considered as large-signal disturbances.

A. Energy-Based Transient Stability Analysis

During each power exchange, the dc voltage $V^j_{\rm dc}$ should be settled on the reference $V^j_{\rm dc,ref}$ in order to form acceptable ac voltages on the BTBC's ac sides (see Fig. 3). Note that tracking the voltage reference should also be in a limited time interval $\Delta T_{\rm stab}$ in which the ac voltages are stable. It is due to the weak MGs voltages and their bad effect on the BTBC performance, which is explained in Section III-C. Otherwise, the BTBC ac voltages will be unstable due to the level difference with MGs voltages (e.g. $V^i_{\rm PCC}$ and V^i_{fc} for VSC$_i$ in Fig. 3). In addition, the assumption of $V^j_{\rm dc0} < V^j_{\rm dc,ref}$ is usually reasonable due to partial capacitor discharges when the BTBC is off. Thus the minimum required energy $W^{\min}_{\rm dc}$ to stabilize the dc voltage before ac voltage instability is as:

$$W^{\min}_{{\rm dc},j} = \frac{1}{2} C^j_{\rm dc} \left({V^j_{\rm dc,ref}}^2 - {V^j_{\rm dc0}}^2 \right) \tag{5}$$

where $V^j_{\rm dc0}$ is the initial dc voltage before power flow change and (5) is based on the well-known capacitor energy relationship. According to the dc voltage controller duty, the VSC$_j$ tries to provide $W^{\min}_{\rm dc}$ by drawing power from the MG$_j$ in $\Delta T_{\rm dc}$. One can give the power-energy relationship as follows:

$$W_{{\rm dc},j} = \int_{\Delta T_{\rm dc}} P_{{\rm dc},j}(t) dt \tag{6}$$

where $\Delta T_{\rm dc}$ is the dc capacitor charging time interval and $P_{{\rm dc},j}$ is the net charging power. As mentioned, in order to preserve stability, the $\Delta T_{\rm dc}$ should be limited to utmost $\Delta T_{\rm stab}$, which is a small time before instability. Therefore, it is easy to recognize $\Delta T_{\rm dc} << 1$, and the average required power can be calculated as

$$P_{{\rm dc},j} = \frac{W_{{\rm dc},j}}{\Delta T_{\rm dc}}. \tag{7}$$

By replacing $W_{{\rm dc},j}$ by its minimum value $W^{\min}_{{\rm dc},j}$ and $\Delta T_{\rm dc}$ by its maximum amount $\Delta T_{\rm stab}$, (7) appears as follows:

$$P_{{\rm dc0},j} \geq \frac{W^{\min}_{{\rm dc},j}}{\Delta T_{\rm stab}} \tag{8}$$

where 0 in subscript indicate the average power required during $\Delta T_{\rm dc}$. By substituting (5) in (8), one can find

$$P^j_{\rm dc0} \geq \frac{1}{2\Delta T_{\rm stab}} C^j_{\rm dc} \left({V^j_{\rm dc,ref}}^2 - {V^j_{\rm dc0}}^2 \right). \tag{9}$$

Then, the $V^j_{\rm dc0}$ can be achieved as follows:

$$V^j_{\rm dc0} \geq \sqrt{{V^j_{\rm dc,ref}}^2 - \frac{2\Delta T_{\rm stab} P^j_{\rm dc0}}{C^j_{\rm dc}}}. \tag{10}$$

This relationship is MSDVC, which shows that the BTBC and generally the IMG system can have a stable operation after enabling the BTBC, if $V^j_{\rm dc0}$ is greater than or equal to a certain value related to $V^j_{\rm dc,ref}$, $\Delta T_{\rm stab}$, $C^j_{\rm dc}$, and $P^j_{\rm dc0}$.

B. MSDVC: Analysis and Discussion

Although the $V^j_{\rm dc,ref}$ in MSDVC (10) is a constant value, other correlated components can change the value of $V^j_{\rm dc0}$ as discussed below. The latest subsection deals with a comparison among MSDVC, CCT, and PTL as common transient assessment tools.

1) Time Interval $\Delta T_{\rm stab}$: The DC-link capacitor voltage has ripples with twice frequency of the ac side [43]. The $V^j_{\rm dc}$ should be stabilized in the first ripples after the event. Otherwise, the ac side voltage disturbance increases and causes instability. In fact, during the stable time interval $\Delta T_{\rm stab}$, the VSC$_j$ output voltage E^j_{C0} should increase to be approximately equal to v^j_{fc}, which is equal to $v^j_{\rm PCC}$ before power exchange. In other words, the stability condition is as

$$E^j_{C0}\Big|_{t \leq \Delta T_{\rm stab}} = v^j_{\rm PCC} \tag{11}$$

where E^j_{C0} and $V^j_{\rm PCC}$ can be obtained as follows [41]:

$$E^j_{C0} = \frac{1}{2} m^j_0 V^j_{\rm dc0} \tag{12a}$$

$$v^j_{\rm PCC} = v^m_o - (R^m_{li} + jL^m_{li}\omega) i^m_o \tag{12b}$$

where m^j_0 is the input control signal of PWM$_j$ during $\Delta T_{\rm stab}$. (12a) is true for three-phase full-bridge converters and (12b) is obtained according to DER$_m$ in MG$_j$ in steady state (see Fig. 2). Note that $v^j_{\rm PCC}$ is an acceptable value less that the nominal ac voltage due to the voltage drop of the DER lines and V-Q droop coefficients.

In stability condition (11), m^j_0 is only variable that can be manipulated to accelerate the increment of E^j_{C0} to be stable. m^j_0 is a function of $\Delta T_{\rm stab}$, which can be found easily according to the dc voltage controller block diagram in Fig. 3. It is obvious that increasing both proportional and integral gains of both current and $v^j_{\rm dc}$ controllers can accelerate the increase of E^j_{C0}. However, such a gain increase is not practical. Because, the gains are limited to the small-signal stability, which is shown in the sensitivity analysis results. Therefore, $\Delta T_{\rm stab}$ is hard to be controlled due

to lack of independent controller. In fact, it is affected by the current and $v_{\rm dc}^j$ controllers, which should be limited for other control/stability objectives. Moreover, according to (12b), MG voltages and currents are as the disturbances for finding $\Delta T_{\rm stab}$. Hence, it is also hard to be calculated. Finally, $\Delta T_{\rm stab}$ cannot be selected neither as a transient stability criteria nor an accessible variable to find easily its impact on MSDVC.

2) Capacitance of the $C_{\rm dc}^j$: It is based on the ability to regulate the dc voltage under transient disturbances. Larger values of $C_{\rm dc}^j$ leads to more required energy to charge it, but the settled voltage is robust against larger disturbances. Therefore, lower values of $C_{\rm dc}^j$ are appropriate in terms of MSDVC. However, the capacitance cannot be selected just based on MSDVC.

3) Injected Power to the dc Link ($P_{\rm dc0}^j$): According to MSDVC, the larger $P_{\rm dc0}^j$ permits the smaller values of $V_{\rm dc0}^j$ to stabilize the dc link voltage. In other words, the $P_{\rm dc0}^j$ increment results in a larger transient stability margin for BTBC-IMGs. According to the active power balance of BTBC dc and ac sides and neglecting switching losses, $P_{\rm dc0}^j$ can be given as follows using Part I relationships [41]:

$$P_{\rm dc0}^j = P_{\rm dc0}^{line} - P_{ji0} = -(P_{\rm dc0}^i + P_{ij0}) - P_{ji0} \tag{13}$$

where $P_{\rm dc0}^{line}$ is the dc line power, $P_{\rm dc0}^i$ is the initial VSC$_i$ capacitor power, and P_{ij0} and P_{ji0} are the VSC$_i$ and VSC$_j$ initial active powers in the ac side, respectively, as shown in Fig. 3, which can be calculated as follows:

$$P_{ij0} = E_{C0}^i i_{IL0}^{ij} = \frac{1}{2} m_0^i V_{\rm dc0}^i i_{IL0}^{ij} \tag{14a}$$

$$P_{ji0} = E_{C0}^j i_{IL0}^{ji} = \frac{1}{2} m_0^j V_{\rm dc0}^j i_{IL0}^{ji} \tag{14b}$$

where ii_{IL0}^{ij} and ii_{IL0}^{ji} are the initial three-phase currents of VSC$_i$ and VSC$_j$, respectively. Regarding (13), (14a), and (14b), following points can be extracted.

i) Terms $P_{\rm dc0}^i$ and P_{ij0} in (13) are as the disturbances in controlling $V_{\rm dc0}^j$. It is reasonable to consider same value and initial condition for both $C_{\rm dc}^i$ and $C_{\rm dc}^i$due to same VSCs and same nominal ac voltages. Therefore, $C_{\rm dc}^i$ needs same initial power, i.e. $P_{\rm dc0}^i = P_{\rm dc0}^j$. As a result, $C_{\rm dc}^i$ cannot be an appropriate contributor in providing $P_{\rm dc0}^j$. However, P_{ij0} can be an effective contributor with a dual behaviour according to the power flow direction, which is illustrated in Section III-D.

ii) Another important point is the presence of $V_{\rm dc0}^j$ in P_{ji0} (14(b)). Although m_0^j is only controllable signal to increase $V_{\rm dc0}^j$, in an instability situation, the term $V_{\rm dc0}^j$ can resonate the instability.

iii) Equations (14a) and (14b), and also, m_i and m_j shown in Fig. 3 express the nonlinear behaviour of the BTBC-IMGs at the beginning of power exchange. Furthermore, they show the complexity and hardness of analytical calculation due to nonlinear relationships and many contributing variables. Hence, the problem of initial BTBC dc voltage in interconnected weak MGs can be listed below the transient stability assessment, which MSDVC is presented for and considered as an appropriate analysis method. Note that enabling BTBC to flow power between MGs is as the large-signal disturbance.

4) MSDVC Comparison With Common Transient Stability Criteria: Generally, the transient stability analysis has been presented for fault occurrence as the common large-signal disturbance. Two common assessment criteria are CCT and PTL. For a fault and given operating condition, CCT is defined as the maximum fault duration, while the power system is still transiently stable [44]. PTL is the maximum power flow through an interface device, e.g. an BTBC, while the power system is still transiently stable. CCT is usually used for ac power flow through ac lines. However, transient stability of dc power exchange through HVDC/BTBC is analyzed by PTL [26]. According to the third point of the previous subsection and definitions of CCT and PTL, it is easy to find their different applications with respect to MSDVC. CCT and PTL have been used to assess the transient stability after a fault occurrence. However, MSDVC is useful to assess the transient stability after a BTBC connection to exchange power.

A relationship can be exist between PTL and MSDVC. In the case of MSDVC application, the initial dc voltage of BTBC is calculated for a given acceptable level of power exchange ($P_{\rm ref}^{ij}$), which is realized by P_{ij0} in (13) and then (10). One can adapt the initial PTL P_{ij0} based on a given $V_{\rm dc0}^j$, which in turn, changes $P_{\rm ref}^{ij}$. In this case, the initial PTL will be the transient stability criterion instead of MSDVC.

In (13), P_{ij0} is the initial power exchange to find the initial PTL and P_{ji0} is a combined impact of the $V_{\rm dc}^j$ controller output ($u_{\rm dc}$) and $-P_{\rm ref}^{ij}$, which is applied by m_0^j. One can find m_0^j according to the dc voltage controller block diagram shown in Fig. 3 and calculate P_{ji0} through (14b). Regarding several multiplications, it is obvious that P_{ji0} is a nonlinear function of the current controller inputs $u_{\rm dc}$ and $-P_{\rm ref}^{ij}$ as follows:

$$P_{ji0} = f_{NL}\left(u_{\rm dc} - P_{\rm ref}^{ij}\right) \tag{15}$$

where NL in the subscript of f indicates its nonlinearity. By substituting (13) and (15) in (9) and rearranging, the initial PTL can be achieved as:

$$P_{ijo} \le \frac{1}{2\Delta T_{\rm stab}} C_{\rm dc}^j \left({V_{\rm dc,ref}^j}^2 - {V_{\rm dc0}^j}^2 \right) + P_{\rm dc0}^i - f_{NL}(u_{\rm dc} - P_{\rm ref}^{ij}). \tag{16}$$

This relation proves an initial PTL for which the BTBC-IMGs remain transiently stable for a given $V_{\rm dc0}^j$.

Note that both MSDVC and initial PTL try to maintain transient stability during BTBC connection. In the case of using MSDVC, the BTBC can be connected with each given power exchange just by pre-charging the dc capacitor to the required dc voltage, and then enabling the BTBC to exchange power. Whereas, by using initial PTL, the initial BTBC power reference is firstly set to be acceptable based on (16) for the given initial dc voltage. After capacitor full-charge, the reference can be modified to the desired value.

C. Grid Strength Impact

It is notable to mention that there is a considerable difference in the case of $P_{\rm dc0}^j$ value between weak VSC-based IMGs and

TABLE I
BACK-TO-BACK CONVERTER POWER EXCHANGE IMPACT ON MSDVC

Situation	P^j_{dc0}	V^j_{dc0}	Stability margin
Power flow from MG_j to MG_i	$S^j_n - S^i_{dc0}$	Increase	Low
Power flow from MG_i to MG_j	$S^j_n + S^i_{dc0}$	Decrease	High
DC voltage stabilization before power exchange	S^j_n	Base case	Medium

strong conventional power grids. After connecting the VSC_j to the MG_j in order to exchange power, the charging power begins to flow from the MG_j into the VSC_j. According to Fig. 3, this power can be calculated as

$$S^j_{ac0} = \left| v^j_{fc,0} \left(\frac{v^j_{fc,0} - E^j_{C0}}{R^j_{fc} + jX^j_{fc}} \right)^* \right| \tag{17}$$

In the most severe case, i.e., $V^j_{\rm dc0} = 0$, the S^j_{ac0} equals to the short circuit level of the power system at the PCC ($S^{pcc}_{SC,j}$). Nevertheless, it equals to the MG_j rating (S^j_n) for weak VSC-based IMGs due to the current-limiting function employed on the DER current controllers. Since $S^{pcc}_{SC,j} >> S^j_n$, the stabilizing initial dc voltage for conventional power systems can be much smaller than VSC-based IMG's one according to the MSDVC. As an important result, the transient stability of initial dc voltage for conventional power systems is less challenging than weak VSC-based IMGs.

D. Power Flow Direction of Back-to-Back Converter

Another important point is the impact of the VSC_i power direction on the MSDVC. Table I shows different situations for the BTBC power flow and their impacts on the MSDVC. In the worst case, where the power should be sent from the MG_j to the MG_i, the net injected power to the dc link is decreased to $S^j_n - S^i_{\rm dc0}$. Thus the stability margin of the $V^j_{\rm dc0}$ is decreased based on the MSDVC. In other words, the $V^j_{\rm dc0}$ should be more close to the $V^j_{\rm dc,ref}$ in order to be stabilize after the transient. In contrast, the net injected power to the dc link is increased to $S^j_n + S^i_{\rm dc0}$ in the case of power transfer from the MG_i to the MG_j. Hence, the stability margin is increased. A third case in Table I is related to enabling the VSC_j before the power exchange. This BTBC operation strategy leads to a medium stability margin in accordance with previous cases.

The transient stability analysis presented in the form of MSDVC is a necessary primary step for designing the dc voltage controller of BTBCs in weak BTBC-IMGs considering the initial dc voltage challenge. The designer can focus on each participant variable, including $\Delta T_{\rm dc}$, $C^j_{\rm dc}$, and $P^j_{\rm dc0}$ to improve the stability. As a simple solution, the dc voltage can be stabilized by enabling $V_{\rm dc}$ controller before power exchange. Another solution is to design a robust dc voltage controller, which can be stable for a range of initial dc voltages as the uncertainty. Note that the control design is outside the scope of this article and can be done in future works.

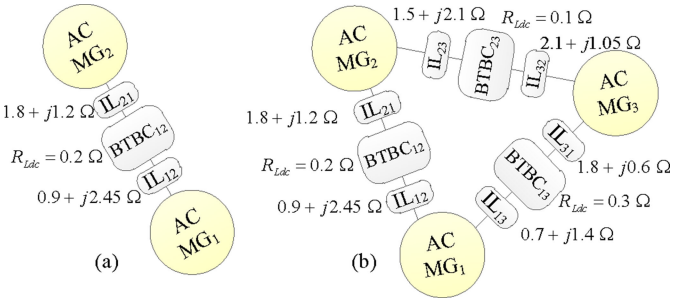

Fig. 4. The structure of the simulated interconnected MGs. (a) Case study 1: two autonomous ac MGs interconnected through one BTBC. (b) Case study 2: three autonomous ac MGs interconnected through three BTBCs.

TABLE II
POWER AND CONTROL DATA OF CASE STUDIES 1 AND 2

Parameters	Symbol	Value					
General features							
Nominal phase voltage	v_n	326 V					
DC link voltage	v_{dc}	780 V					
Nominal frequency	ω_n	100π rad/s					
Back-to-back converters							
DC capacitor	C_{dc}	600 μF					
DC resistance	R_{dc}	0.1 Ω					
CC proportional gain	K^{CC}_p	20					
CC Integral gain	K^{CC}_p	300					
Proportional gain of V_{dc} controller	K^{DVC}_p	5					
Integral gain of V_{dc} controller	K^{DVC}_i	1787					
RLC filter for all converters							
Series inductance	L_f/L_{fc}	1.08/2 mH					
Series resistance	R_f/R_{fc}	0.05/1 Ω					
Shunt capacitance	C_f/C_{fc}	10 μF					
Microgrids							
MG rated power	S_{MG}	3354 VA					
Microgrid number		1		2		3	
Active load (W)		1500		1800		900	
Reactive load (VA)		750		900		450	
DERs		1	2	1	2	1	2
Line ind. (mH)	L_{li}	10.6	5	5	2.5	8.5	4.2
Line res. (Ω)	R_{li}	1.6	0.8	1.2	0.6	1.5	0.7
$\omega - P$ droop gain (rad/kW.s)	m_p	1.6	0.8	1.6	0.8	1.6	0.8
$V - Q$ droop gain (10V/kVAr)	n_q	6.5	3.2	6.5	3.2	6.5	3.2
			K_P				K_I
PI voltage controller			0.05				20
PI current controller			30				500

IV. SIMULATION RESULTS

In this article, two case studies such as an IMG consisting of two autonomous ac MGs interconnected through one BTBC (Case study 1) and an IMG consisting of three autonomous ac MGs interconnected through three BTBCs (Case study 2), shown in 4, are simulated in both Editor/MATLAB and OPAL-RT digital simulator. The details of the real-time OPAL-RT simulator are expressed in Part I [41]. Each MG structure is as shown in Fig. 2. The information of the simulated BTBC-IMGs are presented in Table II, except the interlinking line impedances displayed in Fig. 4. The state matrix $A_{\rm IMG}$ is calculated numerically for both IMGs. A_{2IMG} is a 81×81 matrix and A_{3IMG} is a 159×159 matrix.

TABLE III
PARTICIPATION MATRIX FOR BTBC DC SIDE

State variable	Dynamic modes		
	$\lambda_{23} = -16667$	$\lambda_{70} = j1.05$	$\lambda_{71} = -j1.05$
ΔX_{dc1}	0.5	0.249	0.249
ΔX_{dc2}	0.5	0.249	0.249
ΔX_{DVC}	0	0.499	0.499
Other	0	<0.003	<0.003

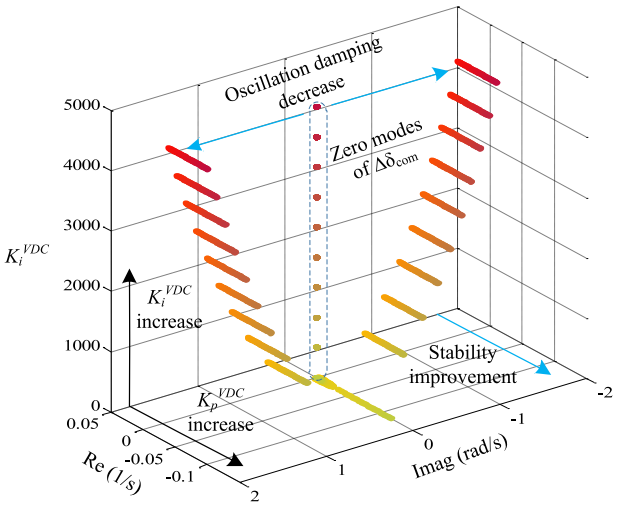

Fig. 5. Sensitivity analysis output for the BTBC voltage controller parameters: $0.1 < K_p^{\mathrm{DVC}} < 200$, $1 < K_i^{\mathrm{DVC}} < 4000$, and $R_{Ldc} = 0$.

Several analyses and simulations are carried out to identify the dynamic behavior of BTBC-IMGs and assess their stability. Using eigenvalue analysis and participation matrix, the impact of each module on the dynamic IMG modes have been specified in Part I [41]. Specially, remarkable contributions of the BTBC parameters e.g. dc voltage controller in the DCMs are identified. Here, sensitivity analysis, as a complementary tool for small-signal stability analysis, is applied on the main participants in the DCMs to find the critical values and acceptable ranges of parameters. Moreover, time-domain simulations verify the theoretical transient stability analysis in Section III, and the sensitivity analysis results in Section IV-A.

A. Sensitivity Analysis

1) DC Side and Voltage Controller of Back-to-Back Converter: Table III shows the participation factors for the dc side and its controller in the Case study 1. The non-dominant mode is only impacted by the dc side parameters. However, the DCMs are related to both power and control parts of the dc link. Fig. 5 indicates the trajectory of the $\lambda_{70,71}$ for changing the dc voltage controller parameters as $0.1 < K_p^{\mathrm{DVC}} < 200$ and $1 < K_i^{\mathrm{DVC}} < 4000$. As a general result, increasing the K_p^{DVC} results in a low stability improvement, and an increase in K_i^{DVC} leads to reduced oscillation damping. In order to maintain stability, the K_p^{DVC} must be chosen larger in relation to a larger K_i^{DVC}. For instance, in the case of $K_i^{\mathrm{DVC}} = 1778$, the dominant frequency modes are stable just for $K_p^{\mathrm{DVC}} > 7.7$. Note that the DCMs are not very sensitive to the dc side elements. However, all resistive elements, e.g. R_{Ldc} improve the stability.

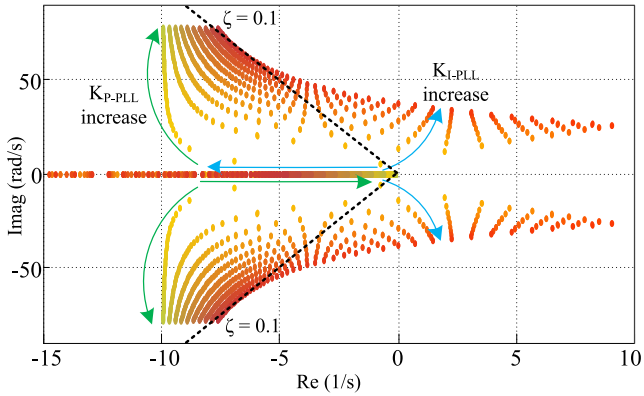

Fig. 6. Sensitivity analysis output for phase-locked loop parameters: $0.01 < K_p^{\mathrm{PLL}} < 1$ and $0.1 < K_i^{\mathrm{PLL}} < 5$.

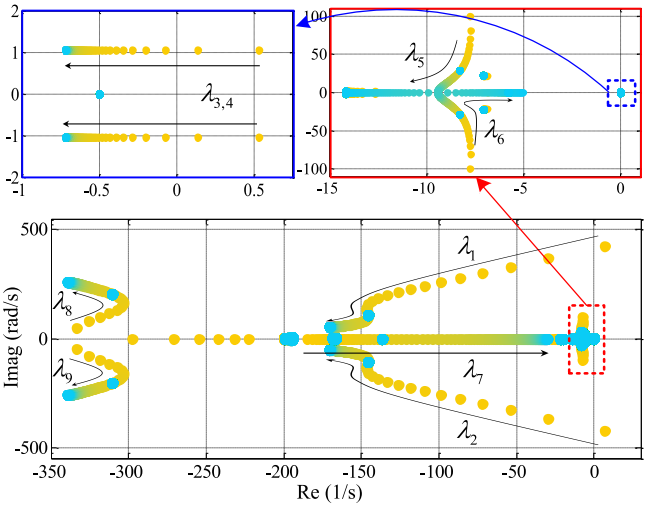

Fig. 7. Sensitivity analysis output for MG2 rating as 335.4 VA $< S_{\mathrm{MG2}} <$ 33.5 kVA, $\Delta V_{\max} = 32.6$ V and $\Delta\omega_{\max} = 1.57$ rad/s.

2) PLLs of Back-to-Back Converter: Fig. 6 shows the loci of BTBC PLL-affected eigenvalues for changing parameters as $0.01 < K_p^{\mathrm{PLL}} < 1$ and $0.1 < K_i^{\mathrm{PLL}} < 5$ in the Case study 1. In accordance with the two oscillatory modes one can conclude: i) when the K_p^{PLL} increases, the stability boundary improves. However, it decreases the oscillation damping for all values of K_i^{PLL}. ii) Very low values of K_p^{PLL} cause instability. iii) The K_i^{PLL} increment causes instability for low K_p^{PLL} values. For the stable non-oscillatory mode, the damping improves by decreasing K_p^{PLL} and/or increasing K_i^{PLL}. In order to satisfy a degree of robust stability and a specified value of the oscillation damping ($\zeta = 0.1$ [12]), acceptable ranges of the PLL parameters can be found, e.g., for Case study 1 as $0.2 \leq K_p^{\mathrm{PLL}} \leq 0.7$ and $0.5 \leq K_i^{\mathrm{PLL}} \leq 2$.

3) $\omega - P$ Droop Characteristic: The m_p changes by DER rating (S_{DER}) variation at a constant $\Delta\omega_{\max}$, which in turn is related to MG rated power (S_{MG}). Fig. 7 shows the DCM trajectories for 335.4 VA $< S_{\mathrm{MG2}} <$ 33.5 kVA and $\Delta\omega_{\max} =$ 1.57 rad/s. S_{MG2} <420 VA causes a severe instability based on $\lambda_{1,2}$ and S_{MG2} <3051 VA ($m_{p1}^{\mathrm{MG2}} > 1.73$ rad/kW.s or $m_{p2}^{\mathrm{MG2}} >$ 0.86 rad/kW.s) causes a very slow instability based on $\lambda_{3,4}$.

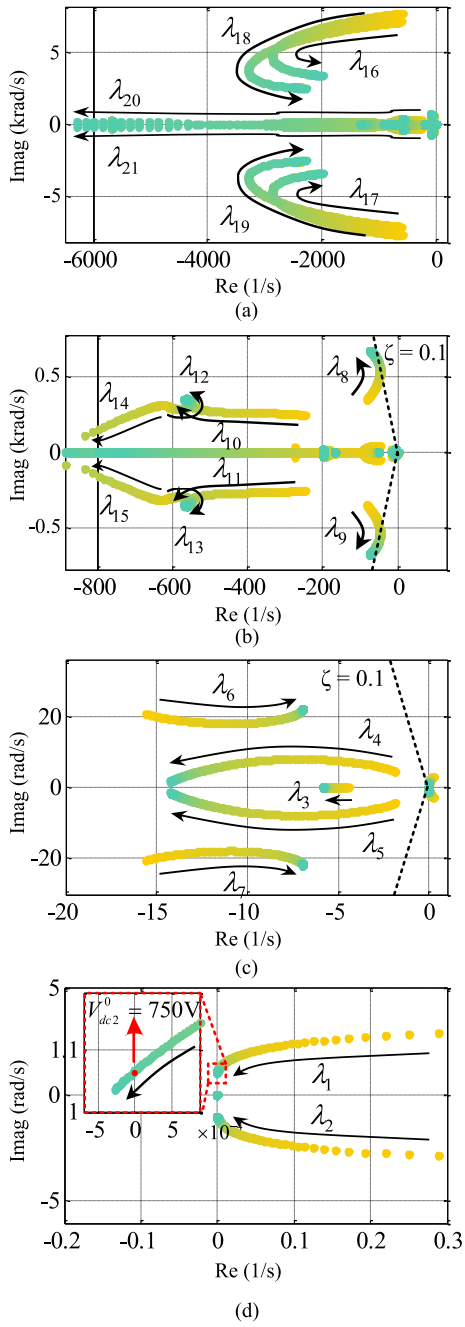

Fig. 8. Sensitivity analysis output for 100 V$< V^0_{\rm dc2} <$800 V in different frequency ranges. (a) Large frequencies. (b) Medium frequencies. (c) Stable low frequency modes. (d) Unstable low-frequency modes for $V^0_{\rm dc2} > 750$.

The droop gain upper limits are already demonstrated for autonomous MGs [45] and CB-IMGs [12], [14].

4) Initial dc Voltage ($V^2_{\rm dc0}$): The $V^2_{\rm dc0}$ should be provided by a supplementary controller e.g. using a parallel battery with $C_{\rm dc2}$, which will be bypassed after precharging. Fig. 8 shows the sensitivity analysis outputs for 100 V$< V^2_{\rm dc0} <$800 V in the Case study 1. According to Fig. 8(a), some medium-frequency modes λ_{16-21} improve the stability by increasing the $V^2_{\rm dc0}$. In addition, improved IMG stability margin can be seen in Fig. 8(b) in accordance with λ_{10-15} by increasing the $V^2_{\rm dc0}$.

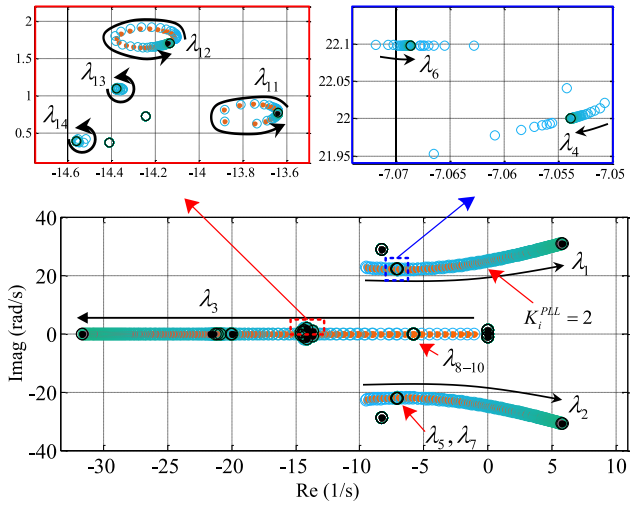

Fig. 9. Sensitivity analysis output when the BTBC$_{12}$'s $K_i^{\rm PLL}$ varies from 0.1 to 5 for Case study 1 (points), and Case study 2 (circles).

Although, the $\lambda_{8,9}$ decrease the system damping. Fig. 8(c) shows the DCMs λ_{3-7}, where are maintained stable for all values of the $V^2_{\rm dc0}$. Nevertheless, the DCMs $\lambda_{1,2}$ can be stable only for $V^2_{\rm dc0} > 750$ V, as shown in Fig. 8(d).

This instability is due to the dc voltage controller inability in charging the $C_{\rm dc2}$ before disturbing the ac sides. In fact, the MSDVC is exceeded. It is noteworthy that the sensitivity analysis outputs in Fig. 8 is not only useful to show the impact of the $V^2_{\rm dc0}$, but also convenient to generally express the participation of the BTBC dc voltage in the IMG stability.

5) Comparison Between Two and Three Interconnected Microgrids: Fig. 9 shows the sensitivity analysis results for changing $K_i^{\rm PLL}$ of BTBC$_{12}$ from 0.1 to 5. In both Case studies 1 and 2, $\lambda_{1,2}$ behave similarly. In the Case study 2, $\lambda_{4,5}$ and $\lambda_{6,7}$, related to BTBC$_{13}$ and BTBC$_{23}$ respectively, have a low tendency to be unstable. The λ_{8-10} are independent from changing the $K_i^{\rm PLL}$ completely and other, λ_{11-14} and their conjugated modes, have a negligible sensitivity to it. Therefore, by changing an effective parameter of one of BTBCs on the DCMs, a considerable interaction cannot be observed among BTBCs themselves and the MGs. In addition, the number of IMGs cannot affect this interaction.

6) Number of Interconnected Microgrids: By increasing the number of IMGs, the structure of the ac passive elements changes and the number of on-mission control instruments increases. According to the eigenvalue analysis and participation matrix results presented in Part I [41], for the case of two IMGs, the ac passive elements e.g. RLC filters, do not have a considerable impact on the DCMs. In addition, parametric changes of the control modules have approximately the same impact on the different number of IMGs. Fig. 9 shows this fact for the Case studies 1 and 2. It can be realized simply for more IMGs using the proposed modeling method. As a pleasant result, the dominant modes are not sensitive to the number of IMGs. On the other hand, increment of on-mission control instruments specially BTBCs leads to an increase in the number of DCMs, which in turn, decreases the IMG security.

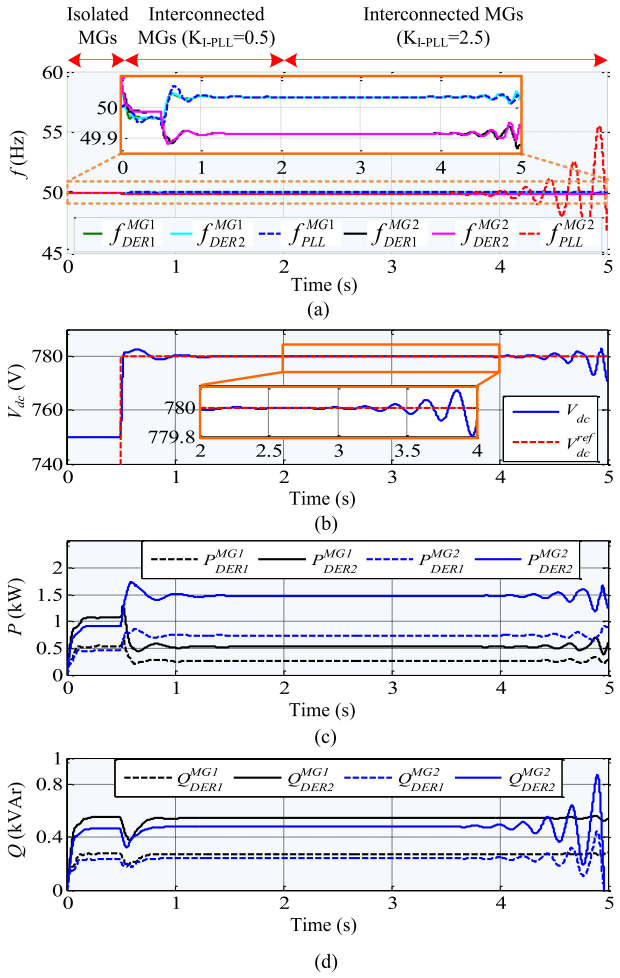

Fig. 10. Case study 1. (a) DER and phase-locked loop frequencies. (b) BTBC_{12} dc voltage. (c) DER's active powers. (d) DER's reactive powers.

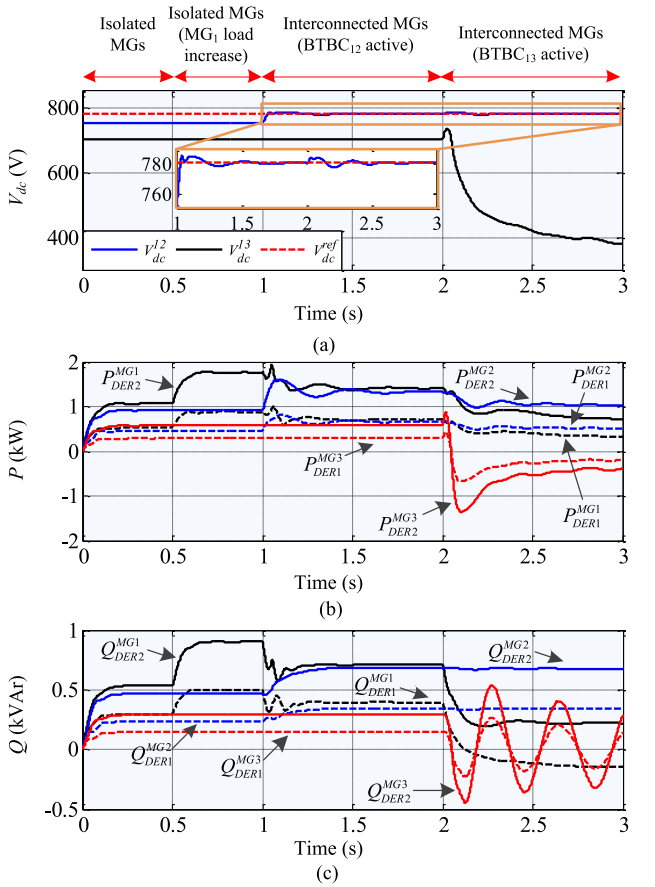

Fig. 11. Case study 2. (a) dc voltage of back-to-back converters. (b) Active powers of DERs. (c) Reactive powers of DERs.

B. Time-Domain Simulations

1) Frequency Instability for Case Study 1: Fig. 10 shows some outputs of the Case study 1, where the MGs are isolated until $t = 0.5$ s. They are connected hereafter with $K_i^{\text{PLL2}} = 0.5$ to exchange 800 W from MG_2 to MG_1, which results in a stable operation. The K_i^{PLL2} is increased to 2.5 at $t = 2$ s. According to Fig. 10(a), DER and PLL frequencies indicate a slow instability due to exciting correlated DCMs to the BTBC_{12} PLL shown in Fig. 6. The instability can be observed in the other measured frequencies with a smaller amplitude, although its amplitude is larger in the $f_{\text{PLL}}^{\text{MG2}}$ itself. The impact of frequency instability on the dc link voltage can be seen in Fig. 10(b), which in turn, spreads the instability to MG_1. Fig. 10(c) and (d) show MG_2 support for MG_1 until $t = 2$ s, then the instability appears. As a result, the obtained ranges for the parameters, e.g. K_i^{PLL2} presented in Section IV-A is necessary to maintain IMG stability.

2) Voltage Instability for Case Study 2: In this scenario, the MGs are isolated at the beginning. The MG_1 load increases at $t = 0.5$ s from 60% to 100% of the rated MG_1 load. MG_2 sends 600 W and 300 VAr to MG_1 at $t = 1$ s via BTBC_{12} while $v_{\text{dc0}}^{12} = 750$ V. MG_3 wants to send 600 W and 300 VAr to MG_1 at $t = 2$ s via BTBC_{13} in order to fully compensate the MG_1 overload, but with $v_{\text{dc0}}^{13} = 700$ V. Since v_{dc0}^{13} is lower than the threshold as 750 V indicated in Fig. 8(d), the v_{dc}^{13} cannot track the reference and goes to a very low value as indicated in Fig. 11(a). The impact of the dc voltage instability on the active and reactive powers of DERs can be observed in Fig. 11(b) and (c). Such a transient voltage instability indicates the necessity of preserving the MSDVC for BTBC-IMGs.

3) Power Flow Direction: As mentioned in Section III-D, the initial dc voltage stability or MSDVC correlates with the BTBC power flow direction. In this scenario, the same power $P_{12}^{\text{ref}} = 855$ W is considered to flow from MG_2 to MG_1 in Situation 1 and from MG_1 to MG_2 in Situation 2. In order to calculate the V_{dc0} stability margin, it is assumed that $R_{\text{dc}} = 0\ \Omega$ and $\Delta T_{\text{dc}} = 0.01$ s. Then, employing (10) and using information in Table II, $V_{\text{dc0}}^{S1} \geq 752.9$ V for Situation 1 and $V_{\text{dc0}}^{S2} \geq 733.7$ V for Situation 2. Therefore, when the power flows from MG_2 to MG_1 as 855 W, the MSDVC equals to 752.9 V, while it is decreased to 733.7 V in Situation 2. For example, $V_{\text{dc0}} = 740$ V can stabilize the two IMGs in Situation 2 [see Fig. 12(a) and (c)], but it cannot stabilize them in Situation 1 [see Fig. 12(a) and (b)]. In Fig. 12, the two MGs are isolated until $t = 1$ s. They are interconnected in the both Situations 1 and 2 at $t = 1$ s. The transient stability is satisfied for Situation 2 due to a stabilizing $V_{\text{dc0}}^{S2} = 740$ V, whereas it cannot be achieved in Situation 1 due to MSDVC violation for the $V_{\text{dc0}}^{S1} = 740$ V. Therefore, the worse power direction must be considered for calculating MSDVC in order to stabilize IMGs under each power flow direction.

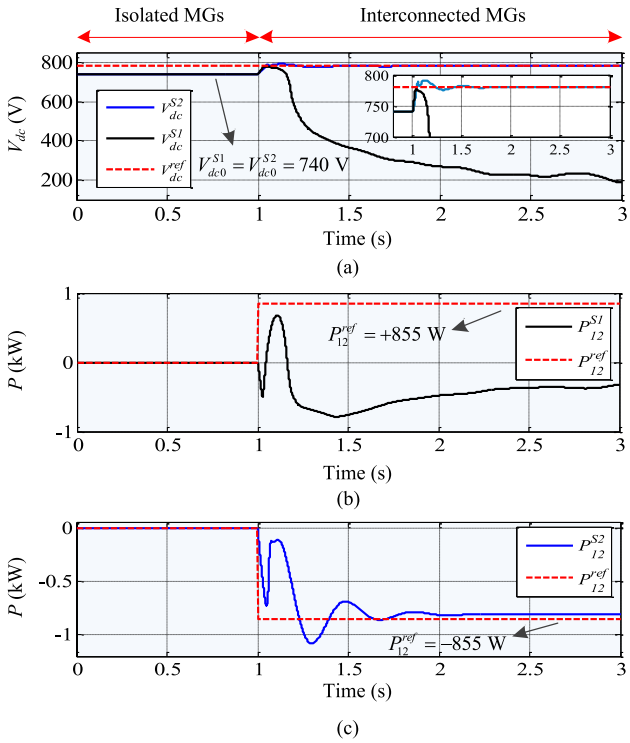

Fig. 12. Impact of the back-to-back converter power flow direction on the transient dc voltage stability. (a) BTBC_{12} dc voltage. (b) Situation 1: power flow from MG_2 to MG_1. (c) Situation 2: power flow from MG_1 to MG_2.

4) Precharging Before Power Flow: As mentioned in Section III-D , precharging the dc capacitor before power flow (base case in Table I) can be as a simple solution for transient stability improvement in the case of enabling BTBC. Similar to the previous Section, the same power $P_{12}^{\mathrm{ref}} = 855$ W is considered to be flown from MG_2 to MG_1 (Situation 1) and from MG_1 to MG_2 (Situation 2) with same $V_{\mathrm{dc0}} = 740$ V. In contrast, the dc capacitor is charged before enabling power flow in [1 2] s for the both Situations. Then, power is flowing in [2 3] s. Fig. 13 shows the transient stability for the both Situations in comparison to Fig. 12, which the dc capacitor is not initially charged. Therefore, pre-charging the dc capacitor has a considerable improvement in the transient stability. Another important observation is decoupling the dynamics of the dc capacitor charge and the power flow. In both Fig. 13(a) and (b), the same dynamics can be seen for the capacitor charging in Situations 1 and 2 during [1 2] s and for the power flow symmetrically during [2 3] s.

5) Initial Power Transfer Limit: Here, initial PTL (IPTL) is considered as the transient stability criterion instead of MSDVC. In the all Scenarios, which applied as power exchange from MG_2 to MG_1 on Case study 1, the MGs are isolated before $t = 1$ s, and then they are interconnected with different V_{dc0} and P_{ref}^{ij}. For $V_{\mathrm{dc0}} = 730$ V, IPTL_1 is obtained as 370 W by increasing P_{ref}^{ij} and checking for the stability. In the first Scenario, $P_{\mathrm{ref}}^{ij} = 114$ W, which is less that IPTL_1. Hence, the dc voltage is transiently stable (Fig. 14(a), blue color), and the active power is settled on the reference after the oscillations [Fig. 14(b), blue color]. In the second Scenario, $P_{\mathrm{ref}}^{ij} = 399$ W, which is a little larger than IPTL_1. Therefore, the dc voltage will be unstable and

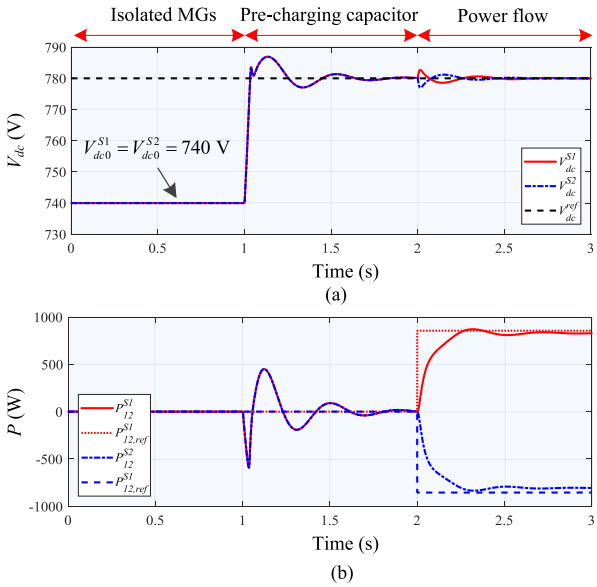

Fig. 13. Pre-charging the BTBC dc capacitor (Case study 1). (a) BTBC_{12} dc voltage. (b) Active power flow for both flow directions from MG_2 to MG_1 (S1), and from MG_1 to MG_2 (S2).

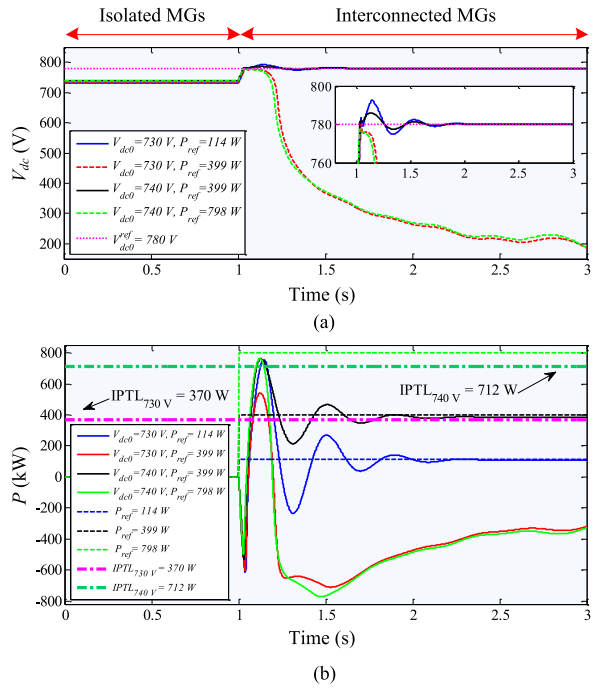

Fig. 14. Initial power transfer limit (IPTL) for two initial dc voltages as 730 and 740 V (Case study 1). (a) BTBC_{12} dc voltage. (b) Active power flow.

the power cannot be stably exchanged (red color). For the same power reference, V_{dc0} is increased to 740 V in the third Scenario. The corresponding IPTL_2 to this new V_{dc0} is found as 712 W. Since $P_{\mathrm{ref}}^{ij} = 399$ W is less than IPTL_2, the stability is preserved in this Scenario (black color). Finally, in order to validate IPTL_2, $P_{\mathrm{ref}}^{ij} = 798$ W>IPTL_2 is considered. The instability can be seen in Fig. 14 (green color). As a result, IPTL can be another criterion of BTBC enabling transient stability, which has a close relation with the initial dc voltage or MSDVC.

V. Conclusion

This article has investigated the stability analysis of fully power-electronics based IMGs comprising VSC-based DERs and power exchanger back-to-back converters. Such IMGs are identified based on the dynamic modes, specially the critical modes. In addition to droop gains, the back-to-back converters parameters are introduced as important participants in the dominant critical modes. According to the sensitivity analysis results, the dc voltage controller parameters, synchronizing PLL parameters and initial dc link voltage are able to destabilize IMGs. In contrast, the passive elements, including interlinking lines and both ac and dc sides of the back-to-back converters do not have a considerable contribution in the critical modes. Thus, the critical mode trajectories do not change remarkably by increasing the number of MGs and their interconnections. Nevertheless, the overall IMG security is reduced owing to the increased number of critical modes.The proposed transient stability assessment for initial dc voltage of the back-to-back converter proves a minimum stabilizing value as the stability margin, which is correlated severely to the power flow direction. As an important result, the back-to-back converters-based IMGs can be operated stable in different situations only by selecting appropriate parameter ranges.

References

[1] R. H. Lasseter, "Smart distribution: Coupled microgrids," *Proc. IEEE*, vol. 99, no. 6, pp. 1074–1082, Jun. 2011.

[2] H. Bevrani, B. François, and T. Ise, *Microgrid Dynamics and Control*. Hoboken, NJ, USA: Wiley, 2017.

[3] D. E. Olivares *et al.*, "Trends in microgrid control," *IEEE Trans. Smart Grid*, vol. 5, no. 4, pp. 1905–1919, Jul. 2014.

[4] Z. Bie, P. Zhang, G. Li, B. Hua, M. Meehan, and X. Wang, "Reliability evaluation of active distribution systems including microgrids," *IEEE Trans. Power Syst.*, vol. 27, no. 4, pp. 2342–2350, Nov. 2012.

[5] F. Katiraei, R. Iravani, N. Hatziargyriou, and A. Dimeas, "Microgrids management," *IEEE Power Energy Mag.*, vol. 6, no. 3, pp. 54–65, May/Jun. 2008.

[6] K. P. Schneider *et al.*, "Improving primary frequency response to support networked microgrid operations," *IEEE Trans. Power Syst.*, vol. 34, no. 1, pp. 659–667, Jan. 2019.

[7] M. Shahidehpour, Z. Li, S. Bahramirad, Z. Li, and W. Tian, "Networked microgrids: Exploring the possibilities of the IIT-bronzeville grid," *IEEE Power Energy Mag.*, vol. 15, no. 4, pp. 63–71, Jul./Aug. 2017.

[8] Y. Zhang, L. Xie, and Q. Ding, "Interactive control of coupled microgrids for guaranteed system-wide small signal stability," *IEEE Trans. Smart Grid*, vol. 7, no. 2, pp. 1088–1096, Mar. 2016.

[9] E. Pashajavid, A. Ghosh, and F. Zare, "A multimode supervisory control scheme for coupling remote droop-regulated microgrids," *IEEE Trans. Smart Grid*, vol. 9, no. 5, pp. 5381–5392, Sep. 2018.

[10] M. J. Hossain, M. A. Mahmud, F. Milano, S. Bacha, and A. Hably, "Design of robust distributed control for interconnected microgrids," *IEEE Trans. Smart Grid*, vol. 7, no. 6, pp. 2724–2735, Nov. 2016.

[11] X. Wu *et al.*, "A two-layer distributed control method for islanded networked microgrid systems," *IEEE Trans. Smart Grid*, vol. 11, no. 2, pp. 942–957, Mar. 2020.

[12] Z. Zhao, P. Yang, Y. Wang, Z. Xu, and J. M. Guerrero, "Dynamic characteristics analysis and stabilization of pv-based multiple microgrid clusters," *IEEE Trans. Smart Grid*, vol. 10, no. 1, pp. 805–818, Jan. 2019.

[13] M. Naderi, Y. Khayat, Q. Shafiee, T. Dragicevic, F. Blaabjerg, and H. Bevrani, "An emergency active and reactive power exchange solution for interconnected microgrids," *IEEE J. Emerging Sel. Topics Power Electron.*, to be published, doi: 10.1109/JESTPE.2019.2954113.

[14] I. P. Nikolakakos *et al.*, "Stability evaluation of interconnected multi-inverter microgrids through critical clusters," *IEEE Trans. Power Syst.*, vol. 31, no. 4, pp. 3060–3072, Jul. 2016.

[15] M. S. Golsorkhi, D. J. Hill, and H. R. Karshenas, "Distributed voltage control and power management of networked microgrids," *IEEE J. Emerg. Sel. Topics Power Electron.*, vol. 6, no. 4, pp. 1892–1902, Dec. 2018.

[16] K. P. Schneider *et al.*, "Enabling resiliency operations across multiple microgrids with grid friendly appliance controllers," *IEEE Trans. Smart Grid*, vol. 9, no. 5, pp. 4755–4764, Sep. 2018.

[17] I. U. Nutkani, P. C. Loh, P. Wang, T. K. Jet, and F. Blaabjerg, "Intertied ac–ac microgrids with autonomous power import and export," *Int. J. Electr. Power Energy Syst.*, vol. 65, pp. 385–393, 2015.

[18] R. Zamora and A. K. Srivastava, "Multi-layer architecture for voltage and frequency control in networked microgrids," *IEEE Trans. Smart Grid*, vol. 9, no. 3, pp. 2076–2085, May 2018.

[19] J. Susanto, F. Shahnia, A. Ghosh, and S. Rajakaruna, "Interconnected microgrids via back-to-back converters for dynamic frequency support," in *Proc. IEEE Power Eng. Conf.*, Sep. 2014, pp. 1–6.

[20] H.-J. Yoo, T.-T. Nguyen, and H.-M. Kim, "Multi-frequency control in a stand-alone multi-microgrid system using a back-to-back converter," *Energies*, vol. 10, no. 6, p. 822, 2017.

[21] N. Flourentzou, V. G. Agelidis, and G. D. Demetriades, "VSC-based HVDC power transmission systems: An overview," *IEEE Trans. Power Electron.*, vol. 24, no. 3, pp. 592–602, Mar. 2009.

[22] A. Yazdani and R. Iravani, *Voltage-Sourced Converters in Power Systems: Modeling, Control, and Applications*. Hoboken, NJ, USA: Wiley, 2010.

[23] J. H. Eto *et al.*, *Use of Frequency Response Metrics to Assess the Planning and Operating Requirements for Reliable Integration of Variable Renewable Generation*. Lawrence Berkeley National Laboratory, 2011.

[24] "IEEE guide for planning dc links terminating at ac locations having low short circuit capacities," IEEE Std. 1204-1997, 1997.

[25] L. Pilotto, M. Szechtman, and A. Hammad, "Transient ac voltage related phenomena for HVdc schemes connected to weak ac systems," *IEEE Trans. Power Del.*, vol. 7, no. 3, pp. 1396–1404, Jul. 1992.

[26] R. Aouini, B. Marinescu, K. B. Kilani, and M. Elleuch, "Stability improvement of the interconnection of weak ac zones by synchronverter-based HVdc link," *Electric Power Syst. Res.*, vol. 142, pp. 112–124, 2017.

[27] H. Latorre and M. Ghandhari, "Improvement of power system stability by using a VSC-HVdc," *Int. J. Electr. Power Energy Syst.*, vol. 33, no. 2, pp. 332–339, 2011.

[28] M. Pavella, D. Ernst, and D. Ruiz-Vega, *Transient Stability of Power Systems: A Unified Approach to Assessment and Control*. New York, USA: Springer Science & Business Media, 2012.

[29] A. Z. Khan and F. Shahzad, "A PC based software package for the equal area criterion of power system transient stability," *IEEE Trans. Power Syst.*, vol. 13, no. 1, pp. 21–26, Feb. 1998.

[30] T. L. Vu and K. Turitsyn, "Lyapunov functions family approach to transient stability assessment," *IEEE Trans. Power Syst.*, vol. 31, no. 2, pp. 1269–1277, Mar. 2016.

[31] J. James, D. J. Hill, A. Y. Lam, J. Gu, and V. O. Li, "Intelligent time-adaptive transient stability assessment system," *IEEE Trans. Power Syst.*, vol. 33, no. 1, pp. 1049–1058, Jan. 2018.

[32] A. K. Alaboudy, H. H. Zeineldin, and J. Kirtley, "Microgrid stability characterization subsequent to fault-triggered islanding incidents," *IEEE Trans. Power Del.*, vol. 27, no. 2, pp. 658–669, Apr. 2012.

[33] J. Alipoor, Y. Miura, and T. Ise, "Stability assessment and optimization methods for microgrid with multiple VSG units," *IEEE Trans. Smart Grid*, vol. 9, no. 2, pp. 1462–1471, Mar. 2018.

[34] Z. Shuai, Y. Hu, Y. Peng, C. Tu, and Z. J. Shen, "Dynamic stability analysis of synchronverter-dominated microgrid based on bifurcation theory," *IEEE Trans. Ind. Electron.*, vol. 64, no. 9, pp. 7467–7477, Sep. 2017.

[35] T.-C. Ou, "A novel unsymmetrical faults analysis for microgrid distribution systems," *Int. J. Electr. Power Energy Syst.*, vol. 43, no. 1, pp. 1017–1024, 2012.

[36] F. Shahnia and A. Arefi, "Eigenanalysis-based small signal stability of the system of coupled sustainable microgrids," *Int. J. Electr. Power Energy Syst.*, vol. 91, pp. 42–60, 2017.

[37] F. Shahnia, "Stability and eigenanalysis of a sustainable remote area microgrid with a transforming structure," *Sustain. Energy Grids Netw.*, vol. 8, pp. 37–50, 2016.

[38] Y. Zhang and L. Xie, "Online dynamic security assessment of microgrid interconnections in smart distribution systems," *IEEE Trans. Power Syst.*, vol. 30, no. 6, pp. 3246–3254, Nov. 2015.

[39] R. Majumder and G. Bag, "Parallel operation of converter interfaced multiple microgrids," *Int. J. Electr. Power Energy Syst.*, vol. 55, pp. 486–496, 2014.

[40] M. Khederzadeh, H. Maleki, and V. Asgharian, "Frequency control improvement of two adjacent microgrids in autonomous mode using back to back voltage-sourced converters," *Int. J. Electr. Power Energy Syst.*, vol. 74, pp. 126–133, 2016.
[41] M. Naderi, Y. Khayat, Q. Shafiee, T. Dragicevic, H. Bevrani, and F. Blaabjerg, "Interconnected autonomous ac microgrids via back-to-back converters–Part I: Small-signal modeling," *IEEE Trans. Power Electron.*, vol. 35, no. 5, pp. 4728–4740, May 2020.
[42] R. Aouini, K. B. Kilani, B. Marinescu, and M. Elleuch, "Improvement of fault critical time by HVdc transmission," in *Proc. 8th Int. Multi-Conf. Syst. Signals Devices*, 2011, pp. 1–6.
[43] M. K. Mishra and K. Karthikeyan, "A fast-acting dc-link voltage controller for three-phase DSTATCOM to compensate ac and dc loads," *IEEE Trans. Power Del.*, vol. 24, no. 4, pp. 2291–2299, Oct. 2009.
[44] P. Kundur, N. J. Balu, and M. G. Lauby, *Power System Stability and Control*. New York, USA: McGraw-Hill, 1994.
[45] N. Pogaku, M. Prodanovic, and T. C. Green, "Modeling, analysis and testing of autonomous operation of an inverter-based microgrid," *IEEE Trans. Power Electron.*, vol. 22, no. 2, pp. 613–625, Mar. 2007.

Mobin Naderi (Student Member, IEEE) was born in Paveh, Iran. He received the B.Sc. degree from Tabriz University, Iran, in 2012, and the M.Sc. degree from the Iran University of Science and Technology, Iran, in 2014, both in electrical engineering, and the Ph.D. degree in the control of modern power systems from University of Kurdistan, Iran, in 2019.

He was a Visiting Ph.D. Student with Department of Energy Technology, Aalborg University, Denmark. His research interests include modeling, stability and control of autonomous and interconnected microgrids.

Yousef Khayat (Student Member, IEEE) received the B.Sc. degree from Urmia University, Urmia, Iran, in 2012, and the M.Sc. degree (hons.) from the Iran University of Science and Technology (IUST), Tehran, Iran, in 2014, both in electrical engineering. He is currently working toward the Ph.D. degree in control of power systems with the University of Kurdistan, Iran.

He is currently a Ph.D. Visiting Student with Aalborg University, Aalborg, Denmark. His research interests include microgrid dynamics and control, robust, predictive and nonlinear control for application of power electronics in distributed systems.

Qobad Shafiee (Senior Member, IEEE) received the Ph.D. degree in electrical engineering from the Department of Energy Technology, Aalborg University, Denmark, in 2014.

He is currently an Assistant Professor, Director of International Relations, and the Program Co-Leader of the Smart/Micro Grids Research Center at the University of Kurdistan, Sanandaj, Iran, where he was a Lecturer from 2007 to 2011. In 2014, he was a Visiting Scholar with the Electrical Engineering Department, the University of Texas at Arlington, Arlington, TX, USA. He was a Post-Doctoral Fellow with the Department of Energy Technology, Aalborg University, in 2015. His current research interests include modeling, energy management, control of power electronics-based systems and microgrids, and model predictive and optimal control of modern power systems.

Tomislav Dragičević (Senior Member, IEEE) received the M.Sc. and the Ph.D. degrees in electrical engineering from the Faculty of Electrical Engineering, University of Zagreb, Croatia, in 2009 and 2013, respectively.

From 2013 until 2016, he was a Postdoctoral researcher at Aalborg University, Denmark. From 2016 to 2020, he was an Associate Professor at Aalborg University, Denmark. Since 2020, he has been a Professor at the Technical University of Denmark. He was a Guest Professor at Nottingham University, UK, during Spring/Summer of 2018. His research interests include application of advanced control, optimization and artificial intelligence inspired techniques to provide innovative and effective solutions to emerging challenges in design, control and cyber-security of power electronics intensive electrical distributions systems and microgrids. He has authored and coauthored more than 200 technical publications (more than 100 of them are published in international journals, mostly in IEEE), eight book chapters, and one book in the field.

He serves as an Associate Editor in the IEEE TRANSACTIONS ON INDUSTRIAL ELECTRONICS, the IEEE TRANSACTIONS ON POWER ELECTRONICS, in IEEE Emerging and Selected Topics in Power Electronics and in IEEE INDUSTRIAL ELECTRONICS MAGAZINE. He is a recipient of the Končar Prize for the Best Industrial Ph.D. thesis in Croatia, a Robert Mayer Energy Conservation Award. He is also a winner of an Alexander von Humboldt Fellowship for experienced researchers.

Hassan Bevrani (Senior Member, IEEE) received Ph.D. degree in electrical engineering from Osaka University, Japan, in 2004.

He is currently a Full Professor and the Program Leader of Smart/Micro Grids Research Center (SMGRC), University of Kurdistan (UOK). From 2016 to 2019, he was the UOK Vice-Chancellor for research and technology. He has also worked as Senior Research Fellow and Visiting Professor with Osaka University, Kumamoto University, Japan; Queensland University of Technology, Australia; Kyushu Institute of Technology, Japan; Centrale Lille, France; and the Technical University of Berlin, Germany. He is the author of six international books, 15 book chapters, and more than 300 journal/conference papers. His current research interests include smart grid operation and control, power systems stability and optimization, microgrid dynamics and control, and Intelligent/robust control applications in power electric industry.

Frede Blaabjerg (Fellow, IEEE) received the Ph.D. degree in electrical engineering from Aalborg University, Denmark, in 1995. He was with ABB-Scandia, Randers, Denmark, from 1987 to 1988. He became an Assistant Professor in 1992, an Associate Professor in 1996, and a Full Professor of power electronics and drives in 1998. In 2017, he became a Villum Investigator. He is honoris causa at University Politehnica Timisoara (UPT), Romania and Tallinn Technical University (TTU), Estonia.

His current research interests include power electronics and its applications such as in wind turbines, PV systems, reliability, harmonics and adjustable speed drives. He has published more than 600 journal papers in the fields of power electronics and its applications. He is the co-author of four monographs and editor of ten books in power electronics and its applications.

He has received 30 IEEE Prize Paper Awards, the IEEE PELS Distinguished Service Award in 2009, the EPE-PEMC Council Award in 2010, the IEEE William E. Newell Power Electronics Award 2014, and the Villum Kann Rasmussen Research Award 2014. He was the Editor-in-Chief of the IEEE TRANSACTIONS ON POWER ELECTRONICS from 2006 to 2012. He has been a Distinguished Lecturer for the IEEE Power Electronics Society, from 2005 to 2007 and for the IEEE Industry Applications Society, from 2010 to 2011 as well as from 2017 to 2018. From 2019 to 2020, he served a President of IEEE Power Electronics Society, and is cuurently the Vice-President of the Danish Academy of Technical Sciences. He was nominated in 2014-2018 by Thomson Reuters to be a the 250 most-cited researchers in engineering in the world.